PART-B

Chapter-5

STUDY OF LOW AND HIGH ENERGY MUONS IN EAS

5.1. Experiment:

In the experiment on simultaneous observation of low and high energy muons, the air shower array set up used is shown in fig.5.1a. The set up has been designed to detect small and medium size air showers with a close-packed array (of spacing 8m.) using an array of 35 scintillation detectors each of size 50cm.X50cm.X5cm., two shielded muon magnet spectrographs (with a spacing of 4m, maximum detectable momentum (MDM) ~500GeV.c^{-1}, each of area 1mX1m. and cut-off at an energy of 2.5GeV.) and a neon flash tube (NFT) chamber as a low energy muon detector. Two spectrographs each with a lever arm of 6.3m. were set up pointing to the zenith to collect muons above 2.5GeV in incident vertical air showers. The array of 35 close-packed plastic scintillation detectors covers an area of ~1200 m^2 at the NBU campus.

For the detection of muons, a telescopic arrangement of scintillation detectors is used. Each magnet spectrograph unit is placed in between scintillation detectors to select the vertical muons passing through it. A two fold coincidence pulse is generated when a muon is passes through the telescope. If this coincidence pulse occurs in coincidence with the air shower trigger, a high voltage pulse of about 4.5KV/cm. of rise time 0.75ms is applied to the electrodes of the neon flash tubes. Four cameras are used for recording the muon trajectory from the flashes of the neon tubes.

5.2. Muon data analysis:

5.2.1. Estimation of muon momentum:

A schematic diagram of the magnet spectrograph, which is used to detect muons in EAS along with the particle trajectory is shown in fig5.2a. The observed muon

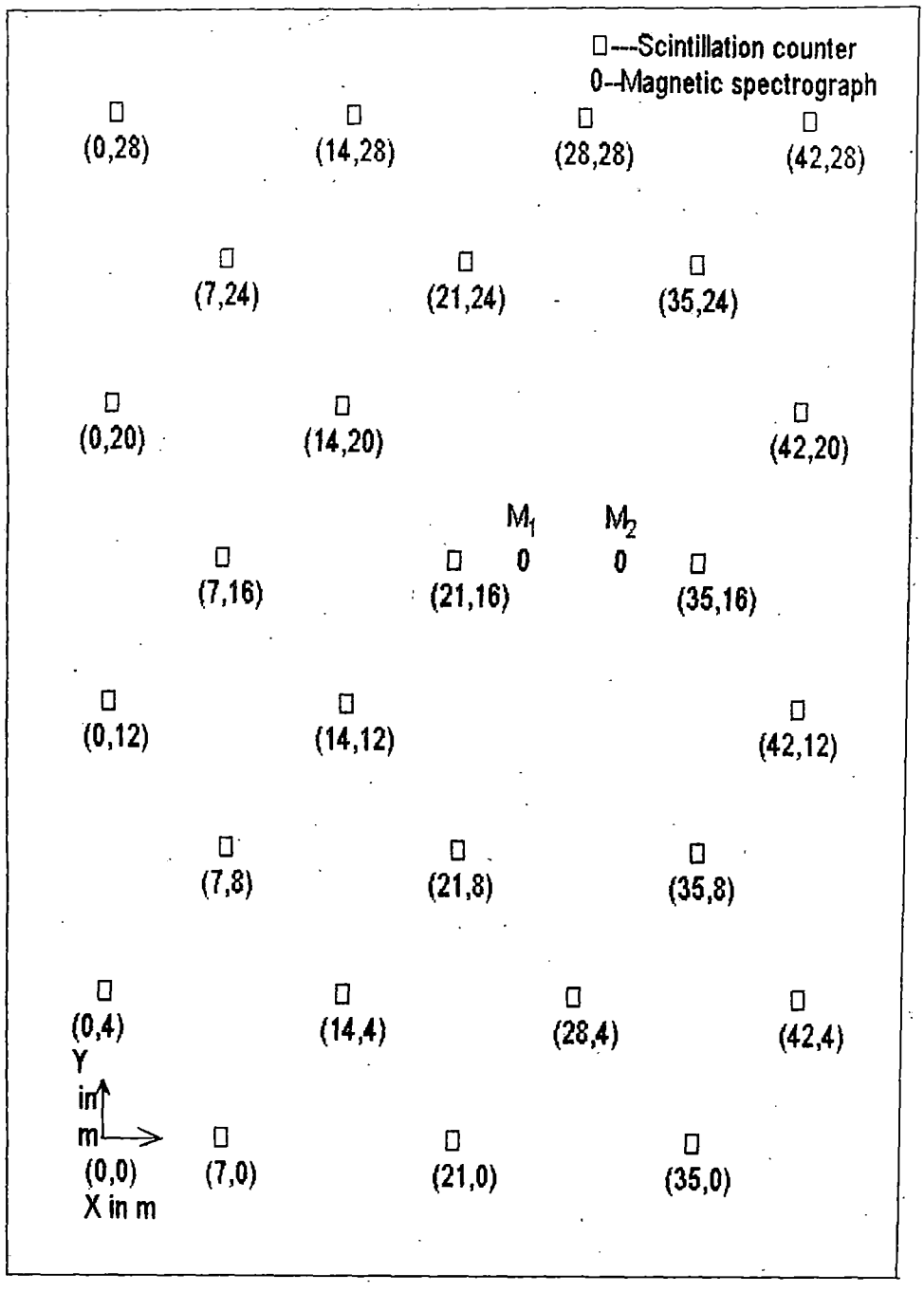

Fig.5.1a.
A diagram of NBU air shower array set up.

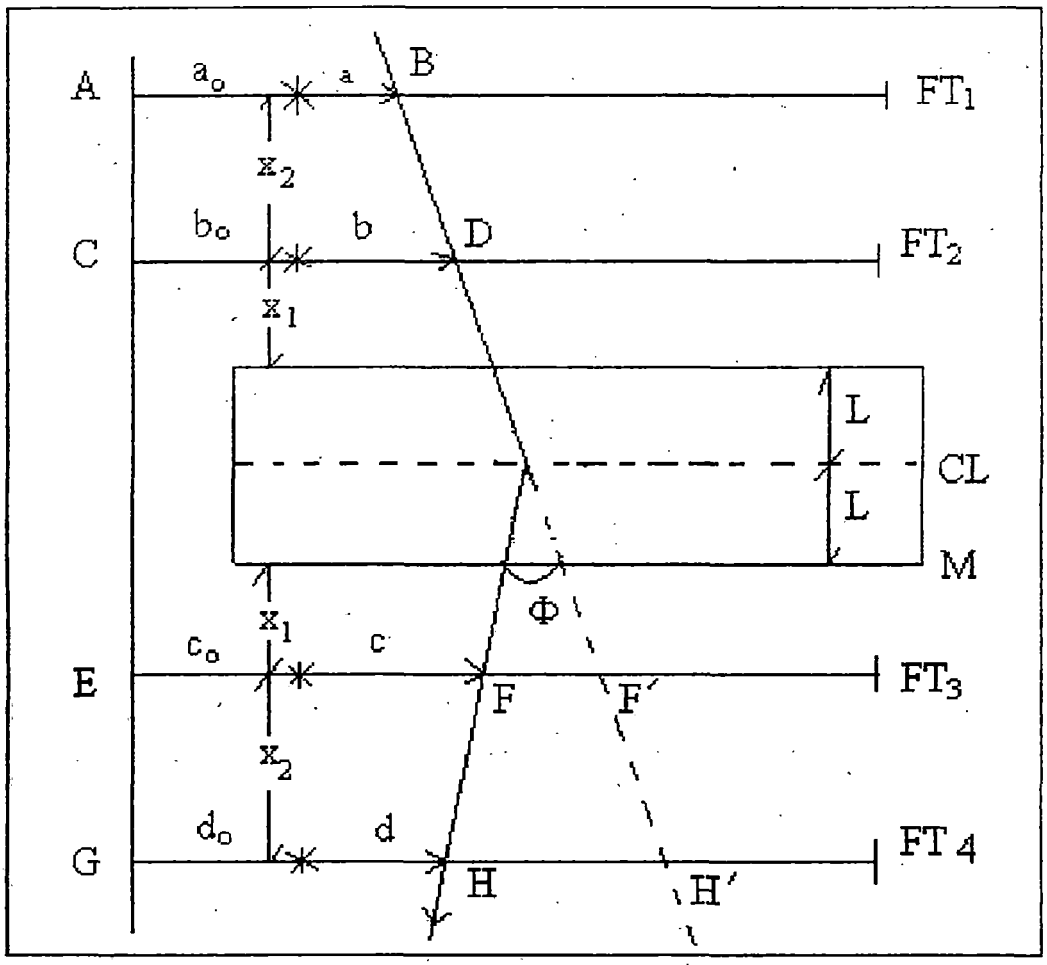

Fig.5.2a.

A schematic diagram of the magnetic spectrograph along with the particle trajectory.

momentum is measured from the deflection in the magnetic field of the spectrogrph as follows.

Let us consider a muon of momentum P and charge e moving transversely through a magnetic field of induction B is related to the radius of curvature ρ of its path given by

$$P = 300.B.\rho \text{ (eV/c)} \quad \text{.....(5.1)}$$

where B is in Gauss and ρ is in cm.

If dl be the length of the element of path traversed by the particle normal to the field and dϕ be the deflection of the muon due to magnetic field, then

$$\rho = dl/d\phi \quad \text{.....(5.2)}$$

Neglecting energy loss in the material of the magnet, the momentum of the muon can be written as

$$P = (300.\int B.dl)/\phi \text{ . (eV/c)} \quad \text{.....(5.3)}$$

where B is in Gauss, l is in cm. and ϕ is in radian.

The deflection in the magnetic field is calculated from the four measured coordinates along the length of the trajectory. In the fig.5.2a, FT_1, FT_2, FT_3 and FT_4 are four neon flash tube trays which determine the muon trajectory. The reference line ACEG is at a distance a_o, b_o, c_o and d_o from the four flash tube trays respectively. CL is the central line of the spectrograph and the effective lenght of the magnet is 2L, where 2L = 106.3cm. x_1,x_2 are the distance of the trays as shown in the fig.5.2a, where $x_1 = 31.85$cm., $x_2 = 85$cm., $L+x_1 = x_2 = 85$cm.

If a perpendicular is drawn from H' on EF' , we get from the geometry of the particle trajectory

$$(GH' - EF')/(FT_3.FT_4) = (CD - AB)/(FT_1.FT_2)$$

Now,

$$[GH + HH' - (EF + FF')]/(FT_3.FT_4) = (CD-AB)/(FT_1.FT_3) \quad .....(5.3)$$

and

$$HH' = \phi\,(L + x_1 + x_2),\ FF' = \phi\,(L + x_1)$$

$$GH' - EF' = (d + d_o) + \phi(L + x_1 + x_2) - (c + c_o) - \phi\,(L + x_1)$$

$$= \phi x_2 + (d + d_o) - (c + c_o)$$

since ϕ is the deflection at the central place of the magnet M. Hence

$$FT_1 \,.\, FT_2 = FT_3 \,.\, FT_4$$

Therefore from equation 5.3, we get

$$\phi x_2 + (d + d_o) - (c + c_o) = (b + b_o) - (a + a_o),$$

$$\phi = [\{(b + b_o) - (a + a_o)\} + \{(c + c_o) - (d + d_o)\}] / x_2$$

$$\text{or, } \phi = (\Delta_o + \Delta_m) / x_2 = \Delta / x_2 \quad .....(5.4)$$

where, $\Delta_o = (b_o - a_o) + (c_o - d_o)$ = geometrical constant of the magnetic spectrograph , $\Delta_m = (b\text{-}a) + (c\text{-}d)$ = geometrical constant due to magnetic deflection and $\Delta = \Delta_o + \Delta_m$.

From equation (5.2) and (5.4), we have

$$P = 300.\int B.dl / \phi$$

$$= 300.B.2L / (\Delta/x_2)$$

$$= 300B \text{ X } 2L \text{ X } x_2 / \Delta = C/\Delta \ (eV/c)$$

where $C = 300B \text{ X } 2L \text{ X } x_2$.

For the NBU magnetic spectrograph,

$B = 1.62X10^4$ G, $2L = 106.3$ cm., $x_2 = 85$ cm.

Therefore, $C = 300 \times 1.62 \times 10^4 \times 106.3 \times 85 / 1.999$ (eV/c) (t.s.)

and $P = 21.96 / \Delta$ (GeV/c) .....(5.5)

where Δ is in tube seperation (t.s.) unit [1 t.s. = (1.999 + 0.0002)cm.].

Thus the momentum can be calculated from equation (5.5) by measuring the quantity Δ.

5.2.2. **Estimation of muon density:**

The average muon density in near vertical showers as a function of the radial coordinate from the shower core was estimated for each of various shower groups in the shower size range 10^4 - 10^6 particles using the average density defined as

$$\rho_\mu (\geq E_\mu, N_e, r) = N_\mu (\geq E_\mu, N_e, r) / [N_t (N_e, r) A']$$

where $N_\mu (\geq E_\mu, N_e, r)$ is the total number of muons recorded in particular distance interval (r) for a particular shower size (N_e) in a certain period of time above a threshold energy ($\geq E_\mu$), $N_t (N_e, r)$ represents the total number of showers of size N_e at the distance interval recorded at the same time and A' is the effective area of the muon detectors.

In a particular shower group, the muons are devided into groups in terms of chosen threshold energies (indicated as $\geq E_\mu$) and then each group is distributed into a number of bins in respect of radial distances from the shower core to determine the average muon density as a function of radial distance and threshold energy.

5.3. **Results:**

The results of the analysis have been incorporated in a paper (accepted in IL NUOVO CIMENTO, date of acceptance Oct.2,1997, Ref. no.7106 NCC), entitled " An experimental study of primary cosmic rays at the knee energy region by observation of Extensive Air Showers (EAS) ", which is presented below.

An experimental study of Primary Cosmic Rays at the knee energy region by observation of Extensive Air Showers (EAS)

G. Saha , A. Bhadra , C. Chakrabarti , S.K. Sarkar and N. Chaudhuri

High Energy and Cosmic Ray Centre , North Bengal University , Darjeeling 734430 , India

Abstract

The simultaneous measurements have been made of the radial (lateral) electron density distribution and the radial muon density distribution at various measured muon energies in the range 2.5-100 GeV in vertically incident EAS in the size range 3.15×10^4-1.79×10^6 (primary energy range 2.4×10^{14} - 8.3×10^{15} eV) particles detected near sea-level. The characteristics of these radial distributions in terms of the measured shower parameters have been determined and used to draw conclusion about the average nuclear mass of the primaries of these EAS.

1. Introduction

It is well established that the Primary Cosmic Ray energy spectrum steepens in the energy range 10^{14} - 10^{16} eV known as the knee energy region .The spectrum steepening is thought to be due to mechanisms related to acceleration and propagation of Primary Cosmic Rays (PCR) .An Extensive Air Shower experiment at primary energy in the knee energy region in which the energy spectrum and lateral distribution of muons can be measured accurately over a wide range can indicate the trend of average behaviour of PCR mass at the knee region . In an EAS of size (N_e) 10^4 - 10^6 particles at sea - level total number of muons and muon lateral distribution ,if the primary is a heavy nucleus , will be different from those in a primary proton initiated shower and the difference can be detected from the data of a properly set-up experiment . In the present paper the results of an air shower experiment covering the knee energy region will be described . This experiment with the provision for differential measurement of both low and high energy muons simultaneously by two shielded magnet spectrographs has yielded both muon energy spectrum and radial density distributions at various muon energies. The properties of these distributions have been analysed to infer the trend of average PCR mass composition at the knee region.

2. North Bengal University (N.B.U) air shower experiment

The North Bengal University EAS array for observation of air showers has been developed in stages since 1980 (Basak et al [1]). The set-up has been designed to detect small and medium size air showers with a close -packed array (of spacing 8m) using an array of 35 scintillation detectors each of size 50 cm x 50 cm, two shielded muon magnet spectrographs (with a spacing of 4m, maximum

detectable momentum (MDM) 500 GeV c^{-1}, each of area 1m x 1m and cut off at an energy of 2.5 GeV) and a nuon flash tube (NFT) chamber as a low energy muon detector. Two spectrographs each with a lever arm of 6.3m were set up pointing to the zenith to collect muons above 2.5 GeV in incident vertical air showers. With such a close-packed array , the determination of shower size and other shower parameters has been more precise.

2·1. EAS detector array characteristics

The array of 35 close-packed plastic scintillation detectors (Fig.1) has been operating at a site of atmospheric depth ~ 1000 gcm^{-2} at the N.B.U campus. The response measured in terms of the relative light output of plastic scintillator (manufactured by Bhabha Atomic Research Centre, India) for incident EAS electrons is ~ 100% and the relative efficiency in terms of single particle pulse height is nearly uniform from centre to edge of each plastic scintillation detector. The pulses from all the 35 scintillation detectors are digitized by an analog to digital converter one after the other and connected to the memory unit for storing the digital information and subsequent transfer to the printer for printing on a paper tape. The printed outputs give the information about the particle densities on each detector in an individual shower.

The efficiency of detecting showers of different N_e and age(s) within the sensitive detecting area of ~1200 m^2 and the average triggering probability of the array for showers falling within 15^0 of the zenith are shown in figs. 2,3,4,5 and 6.

Two magnetic spectrographs and the NFT chamber were operated under an EAS trigger which was also used for the photographic recording of muon trajectories within a track location uncertainty of ± 0.14 cm.

The selection criteria for shower detection consists of the following steps:

(1) Shower is recorded by the detecting system if the registered electron density in any four adjacent detectors of the 8 central triggering detectors is greater than 4 particles/m^2 .

(2) The electron densities at 19 points are registered simultaneously with the phptographic recording of the trajectories of muons by the two spectrographs at four points in individual shower.

(3) For each recorded shower ,the core location , the shower size and the photon electron cascade age (s) of the EAS are determined by fitting the registered electron densities with the following formula for the electron density $\Delta(r)$

$$\Delta(r) = N_e/r_1^2[\, f(r/r_1,s)\,] \qquad \ldots\ldots\ldots\ldots\ldots\ldots (1)$$

where $f(r/r_1, s) = c(s)\,(r/r_1)^{a1+a2(s-1)}\,(1+r/r_1)^{b1+b2(s-1)}$

c(s) is the normalisation constant , r_1= 24 m (Moliere unit of displacement at sea-level) and a1,a2,b1,b2 are constants . Some examples of average radial electron density distributions at N_e= 1.09×10^5 - 1.79×10^6 particles together with the graphs of fitting function are shown in Fig.7. The shower size recorded by the array is 3.15×10^4 - 1.79×10^6 particles .

3. Analysis and error estimation .

A standard χ^2 - minimization procedure based on the method of steepest descent has been used to determine the air shower parameters and to simulate the errors in the air shower parameters.

The errors in the determination of EAS parameters have been evaluated through the standard procedure of artificial shower analysis. A shower of known parameters is allowed to be incident at any point on the array selected at random and particle density in each detector is calculated according to the chosen lateral distribution function. To reproduce the experimental conditions, the statistical fluctuations in the number of particles in each detector and the systemetic errors in the conversion of pulse height into particle density are superposed on each density.For a set of densities for each shower,χ^2 - minimization procedure is applied to estimate the shower parameters . The estimated shower parameters give the deviations from the actual ones used for an artificial shower and lead to the following error estimates :

(1) ΔX = 2.40m
ΔY = 2.77m

(2) $\Delta N_e/N_e$ = 9.61%

(3) ΔS = .13

Some histograms for the deviations of the parameters are shown in Fig. 8.

4. Results on ' near vertical showers'

4·1. Determination of shower age (s) and energy of the shower.

Using all the registered electron densities in a shower event the best fitted value of the shower age(s) was determined by the method of least square. For each shower of fixed size and age (s)

the mean energy of the primary particle (proton) was obtained with a maximum error of 10% (which includes fluctuation in EAS development and the error in shower size measurement) from the energy scale established on the basis of hybrid Monte Carlo model (Trzupek et al [2]) for EAS at sea-level as given by

$$E_0\,(eV) = 3.03\times10^{10}\times N_e^{0.87} \quad \ldots\ldots\ldots\ldots\ldots\ldots\ldots\ldots\ldots\ldots (2)$$

4·2. Measurement of muon density

The average muon density in a shower as a function of the radial distance from the shower core was estimated for each of the various shower groups in the shower size range 3.15×10^4 - 1.79×10^6 particles using the average density defined as

$$\rho_\mu(\geq E_\mu, N_e(s), r) = N\mu(\geq E\mu, N_e(s), r) \,/\, N_t(N_e(s), r)\, A' \quad \ldots\ldots\ldots (3)$$

Where $N\mu(\geq E\mu, N_e(s), r)$is the total number of muons recorded in a particular distance r for a particular shower size N_e in a certain period of time above a threshold energy ($\geq E\mu$), $N_t(N_e(s), r)$ represents the total number of showers of size $N_e(s)$ at the same distance interval recorded at the same time and A' is the effective area of the muon detectors .

In a particular shower size group the muons are divided into groups on the basis of specified threshold energies (indicated as $\geq E\mu$) and then each group is distributed into a number of bins in respect of radial distances from the shower core to determine the average muon density as a function of radial distance and threshold energy.

Some results on muon energy spectra and lateral distributions are given in Figs. 9 and 10 .

4·3. The dependence of muon density on shower size and radial distance

The variation of muon density at fixed radial distances has been studied as a function of shower size at various muon threshold energies by assuming a dependence of the form given by

$$\rho_\mu(\geq E\mu\,, r) \sim N_e{}^{\beta(E\mu, r)} \quad \ldots\ldots\ldots\ldots\ldots\ldots\ldots\ldots\ldots (4)$$

The fit to the observed data has yielded the results shown in Figs. 11,12 and 13.It is seen that at a fixed muon threshold energy β decreases slowly with radial distance for all shower sizes in the range 3.15×10^4 - 1.79×10^6 particles and the trend of variation of β with radial distance is similar for all muon threshold energies . All these results together seem to indicate that the muon distribution function does not change with primary energy .The values of the exponent (β) obtained by fitting the observed data are given in table 1.

Table 1. Values of the exponent β at different distance ranges for various muon energies

Muon Energy (GeV)	Value of β (for r=8-12m)	Value of β (for r=30-40m)
2.5	0.692±0.009	0.653±0.012
10	0.699±0.010	0.655±0.013
50	0.661±0.011	0.587±0.021

The measured lateral distribution of muons in showers of various sizes are fitted to a relation of the form

$$\rho_\mu (\geq E_\mu, r, N_e) \sim r^{-\alpha(\geq E\mu)} \quad \ldots\ldots\ldots\ldots\ldots\ldots (5)$$

A plot of this function for $N_e = 4.48 \times 10^5$ and $E_\mu \geq 2.5$ GeV is shown in fig. 14 as an example . The value of α derived from this plot is 0.647.The least-square fitted line obtained from the plot of log ρ_μ vs. log r at fixed N_e and E_μ gives the value of α . To determine such values of α the shower cores except for the last radial bin (as for an example r=34.1m shown in fig.14) were taken inside the edges of the array where the efficiency of the array is large . For the last radial bin , which is also close to the array boundary , obviously the error of r and N_e are comparatively large but the overall effect of these errors on determination of α is small .The mean values of α with r.m.s errors for $E_\mu \geq 2.5$ GeV are given in table 2.

Values of α from the fit of the data for $E_\mu \geq 2.5$ GeV are shown as a function of N_e in Fig. 15. The trend of α vs E_o curve shows that α is a function of energy upto 4.6×10^{15} eV and becomes constant at higher energies. The lateral muon density distribution in a shower initiated by a heavy primary is flatter compared to the corresponding one initiated by a lighter primary at the same energy . In other wards for a lighter primary composition it is expected to have steeper muon lateral distribution and hence a large value of α .Therefore the variation of α with E_o as shown in fig.15 possibly indicates that the effective primary mass is decreasing with energy increasing from 4.3×10^{14} eV to around 4.6×10^{15}eV

Table 2. Values of the exponent α for various shower sizes at muon threshold energy ($\geq E_\mu$) 2.5 GeV

Shower size	$\alpha \pm d\alpha$
5.97×10^4	0.553±0.009
1.09×10^5	0.578±0.010
2.21×10^5	0.606±0.012
4.48×10^5	0.647±0.014
9.02×10^5	0.661±0.016
1.79×10^6	0.662±0.016

5. Discussion

The method used in the present analysis consists of examining the accurately measured muon densities as a function of shower size and the muon lateral distribution (for various muon threshold energies) as a function of shower size .The analysis also includes the results of an estimation of errors to the EAS parameters . The primary energy of an EAS event is not possible to be determined precisely from the observed particle density distribution due to the presence of fluctuations in an EAS development .However the mean primary energy range (2.4×10^{14}-8.3×10^{15} eV) concerned in the present experiment was determined by comparing the observed vertical shower size with the results of hybrid Monte Carlo model for proton primary at sea-level covering this primary energy range. Some representative examples of measured muon energy spectra and radial distributions are presented in Figs. 9 and 10 to show that these provide a firm experimental base for comparing with different models of EAS. An analysis of these results given in section 4.3 leads to the following conclusion :

The radial muon density distribution at low and high muon energies does not change with the primary energy

For low energy muons radial muon density distribution steepens in the primary energy range 4.3×10^{14} - 4.6×10^{15} eV with radial distance (r) indicating that the effective primary mass decreasing between 4.3×10^{14} - 4.6×10^{15} eV.

Y.Kawamura et al [3] and M.Ichimura et al [4] have derived similar conclusion about primary mass in the knee energy region from direct observations from their new emulsion chamber experiments . From an analysis of low energy EAS muons Blake et al [5] reported similar trend for average primary mass in the primary energy region 6.0×10^{14} - 5×10^{15} eV.

This work is being continued to improve statistics on this aspect of study using muon lateral distributions at different energies of muons in EAS. The existing array is being expanded to operate at larger shower sizes so that the present method of analysis can be applied under better accuracies on the determination of EAS parameters.

Reference

(1) Basak D.K.,Chakraborti N.,Ghosh B.,Goswami G.C. and Chaudhuri N. (1984). Nucl.Instrum.Methods 227,167

(2) Trzupek A.,Lu Y. and Poirier J. (1993), 23rd ICRC , Calgary , Vol.4, p. 359

(3) Kawamura Y. et al (1989) . Phy.Rev. D40,729

(4) Ichimura M. et al (1992) , ICRR Report 287, 92-95

(5) Blake P.R and Tummey S.P. (1993), 23rd ICRC ,Calgary,Vol.4, p.363

Figure captions

Fig.1. A diagram of N.B.U air shower array set-up

Fig.2. The efficiency of detection of the array as a function of distance from the centre of the array for s= 1.2 and $N_e = 8x10^4$

Fig.3. Same as in Fig.2 but for $N_e = 10^5$

Fig.4. Same as in Fig.2 but for $N_e = 5x10^5$

Fig.5. Same as in Fig.2 but for $N_e = 10^6$

Fig.6. The average triggering probability for the array of detectors as a function of shower size for core distances at 20m,30m and 40m

Fig.7. Plots of lateral electron density distribution at shower size $1.09x10^5$-$1.79x10^6$ with shower age (s) = 1.2

Fig.8. Error distribution in core location ,shower size and age parameter.

Fig.9. Variation of muon density with muon energy at various radial distances.

Fig.10. Lateral muon density distribution at the threshold energy of 2.5 GeV for showers of size range $5.97x10^4$ - $9.02x10^5$ of s =1.2

Fig.11. Variation of muon density at radial distance ranges 8-12m and 30-40m with shower size at muon threshold ($\geq E_\mu$) energy 2.5 GeV

Fig.12. Same as in Fig.11 but for muon threshold ($\geq E_\mu$) energy 10 GeV

Fig.13. Same as in Fig.11 but for muon threshold ($\geq E_\mu$) energy 50 Gev

Fig.14. Variation of muon density with radial distance for $N_e=4.48x10^5$

Fig.15. Variation of α with shower size (N_e) at the muon threshold ($\geq E_\mu$) energy 2.5 GeV

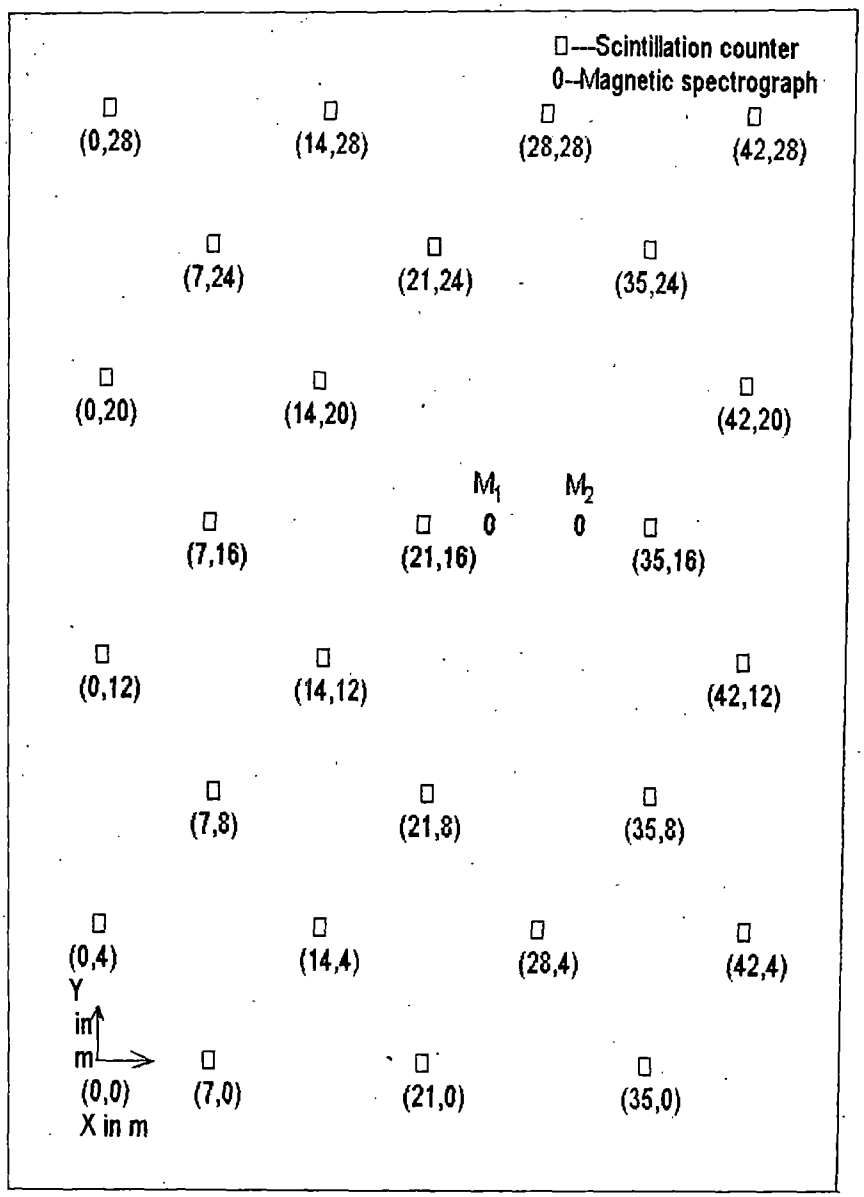
□---Scintillation counter
0--Magnetic spectrograph
(0,28)
(14,28)
(28,28)
(42,28)
(7,24)
(21,24)
(35,24)
(0,20)
(14,20)
(42,20)
M1
M2
0
0
(7,16)
(21,16)
(35,16)
(0,12)
(14,12)
(42,12)
(7,8)
(21,8)
(35,8)
(0,4)
(14,4)
(28,4)
(42,4)
Y in m
(0,0)
X in m
(7,0)
(21,0)
(35,0)

Fig.1

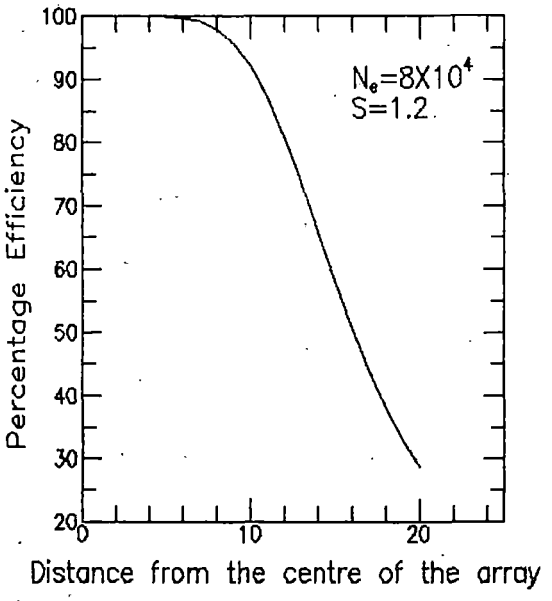

Fig.2

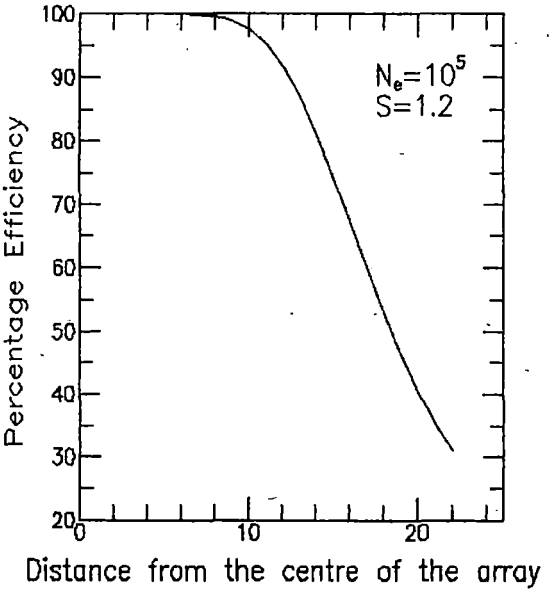

Fig.3

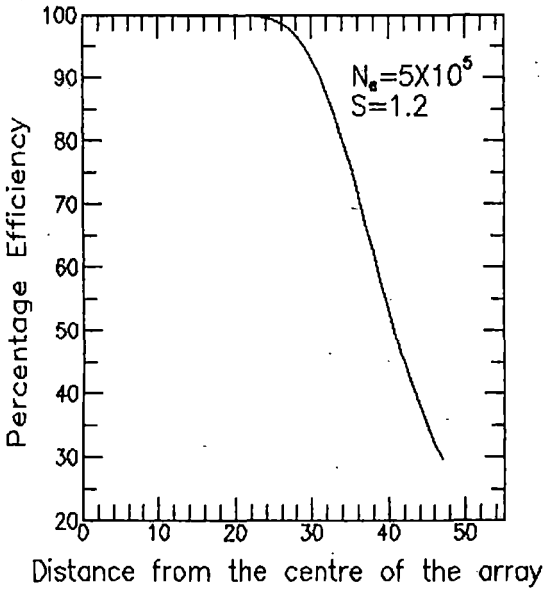

Fig.4

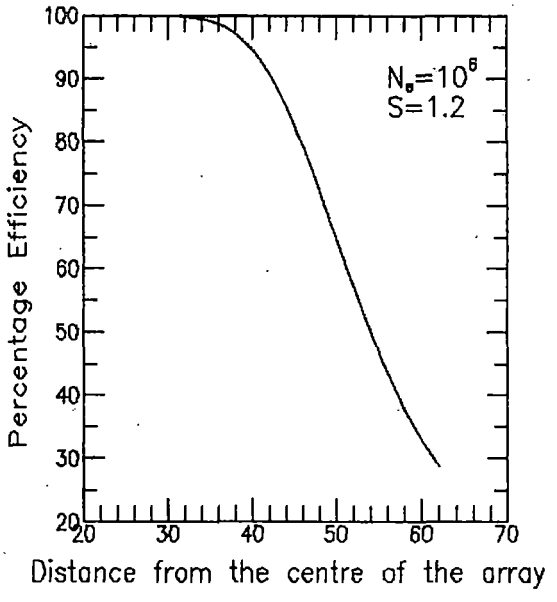

Fig.5

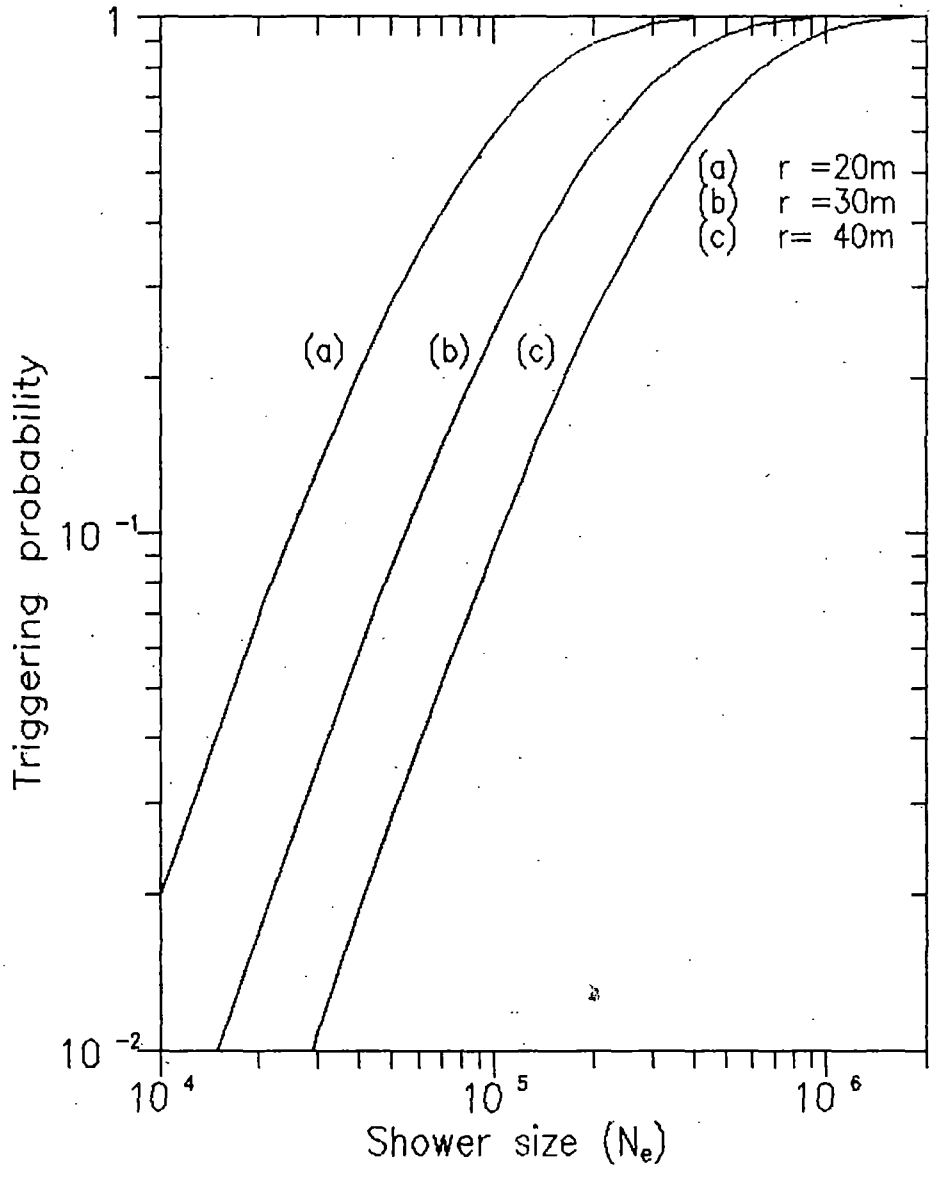
1
10^{-1}
10^{-2}
10^{4}
10^{5}
10^{6}
Triggering probability
Shower size (N_e)
(a) r =20m
(b) r =30m
(c) r= 40m
(a)
(b)
(c)

Fig.6

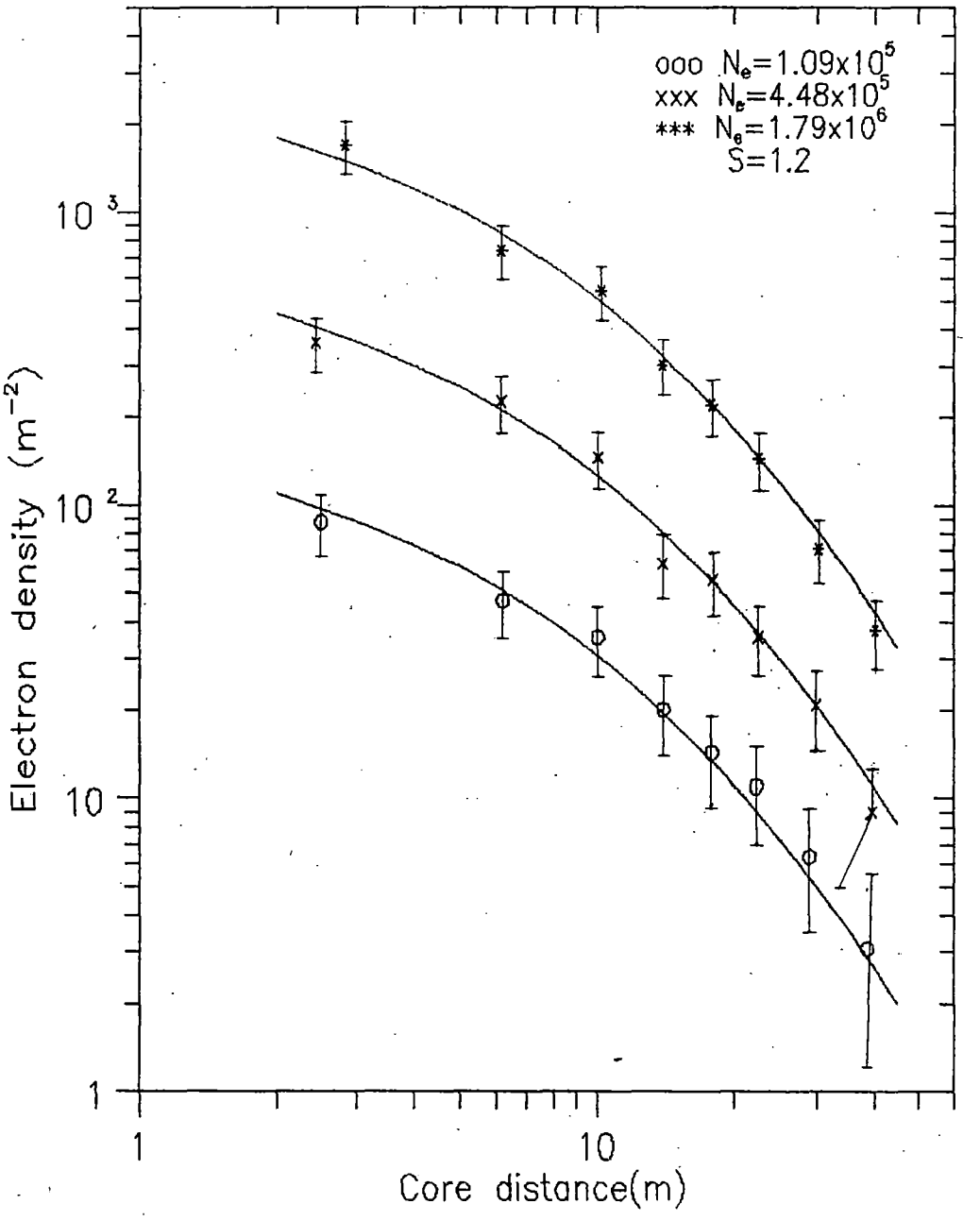
ooo N_e=1.09x10^5
xxx N_e=4.48x10^5
*** N_e=1.79x10^6
S=1.2
Electron density (m^{-2})
10^3
10^2
10
1
1
10
Core distance(m)

Fig.7

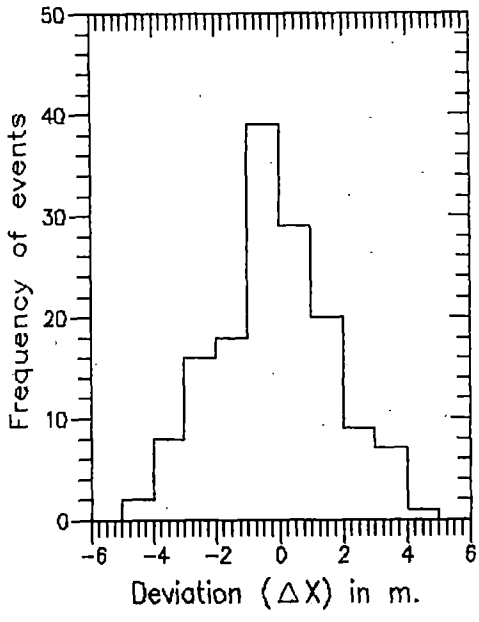
Frequency of events
Deviation (ΔX) in m.

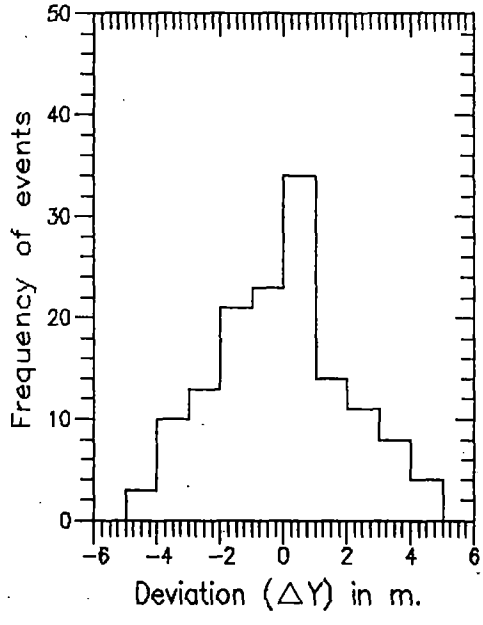
Frequency of events
Deviation (ΔY) in m.

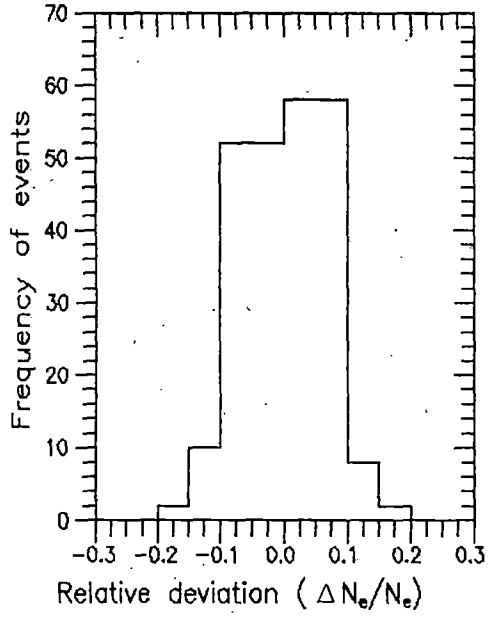
Frequency of events
Relative deviation (ΔNe/Ne)

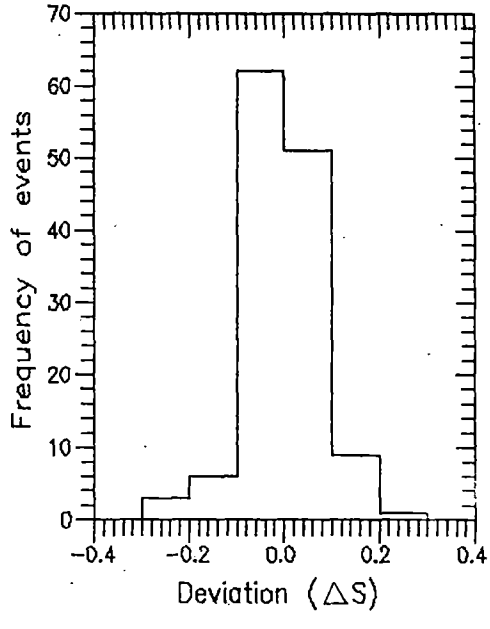
Frequency of events
Deviation (ΔS)

Fig.8

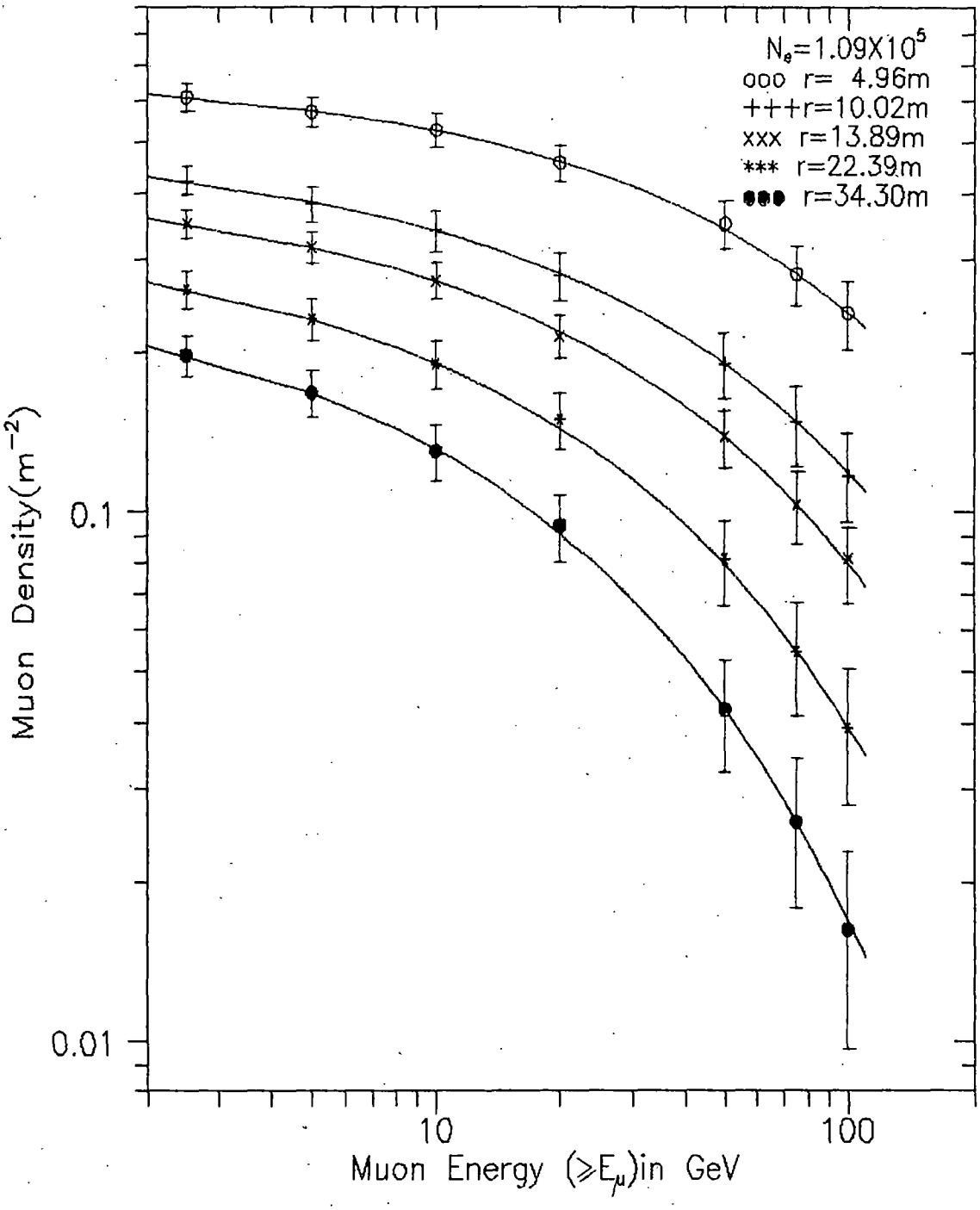
N_e=1.09X10^5
ooo r= 4.96m
+++r=10.02m
xxx r=13.89m
*** r=22.39m
●●● r=34.30m
Muon Density(m^{-2})
0.1
0.01
10
100
Muon Energy (≥E_μ)in GeV

Fig.9

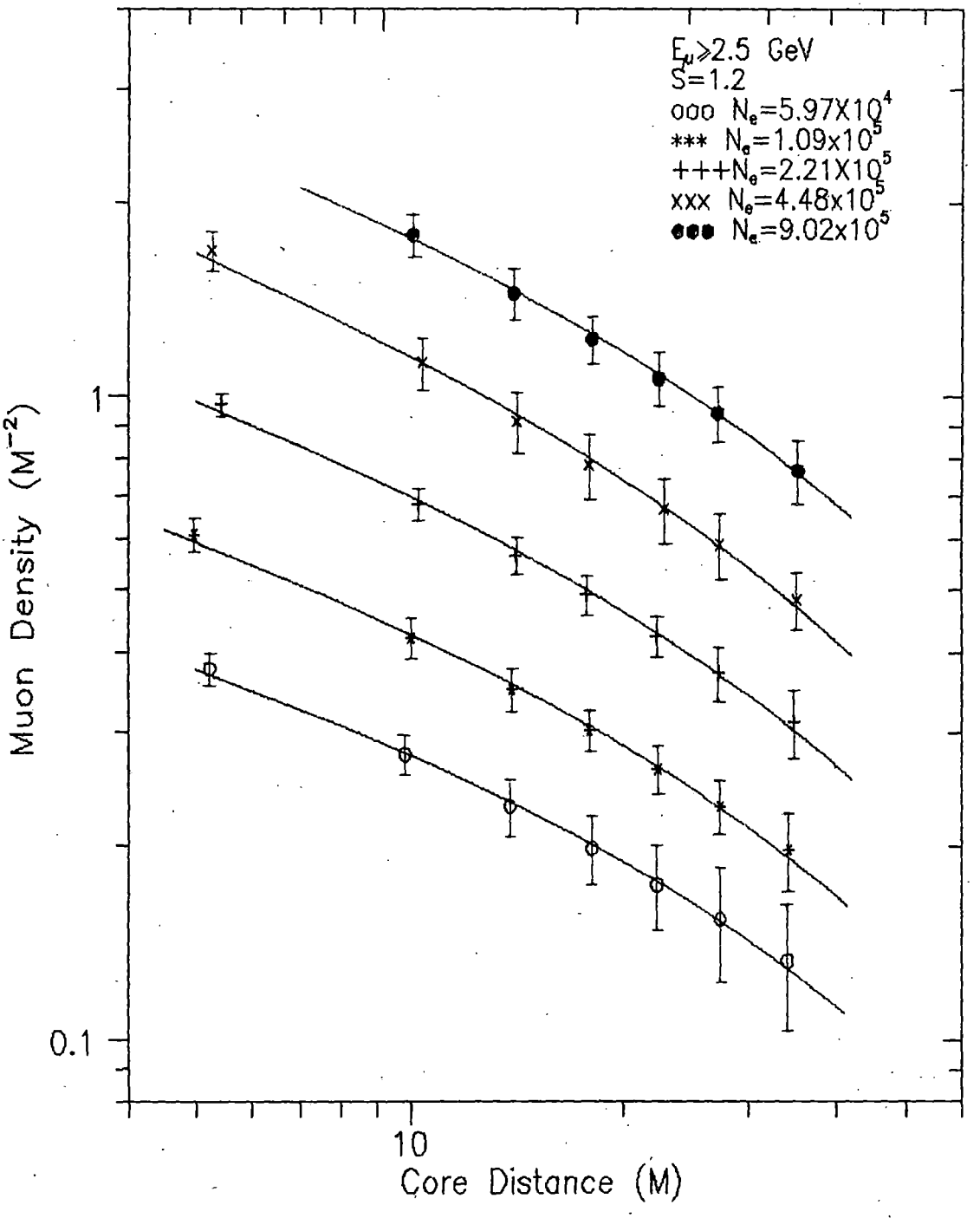
$E_\mu \geq 2.5$ GeV
S=1.2
ooo N_e=5.97X10^4
*** N_e=1.09x10^5
+++N_e=2.21X10^5
xxx N_e=4.48x10^5
●●● N_e=9.02x10^5
Muon Density (M^{-2})
1
0.1
10
Core Distance (M)

Fig.10

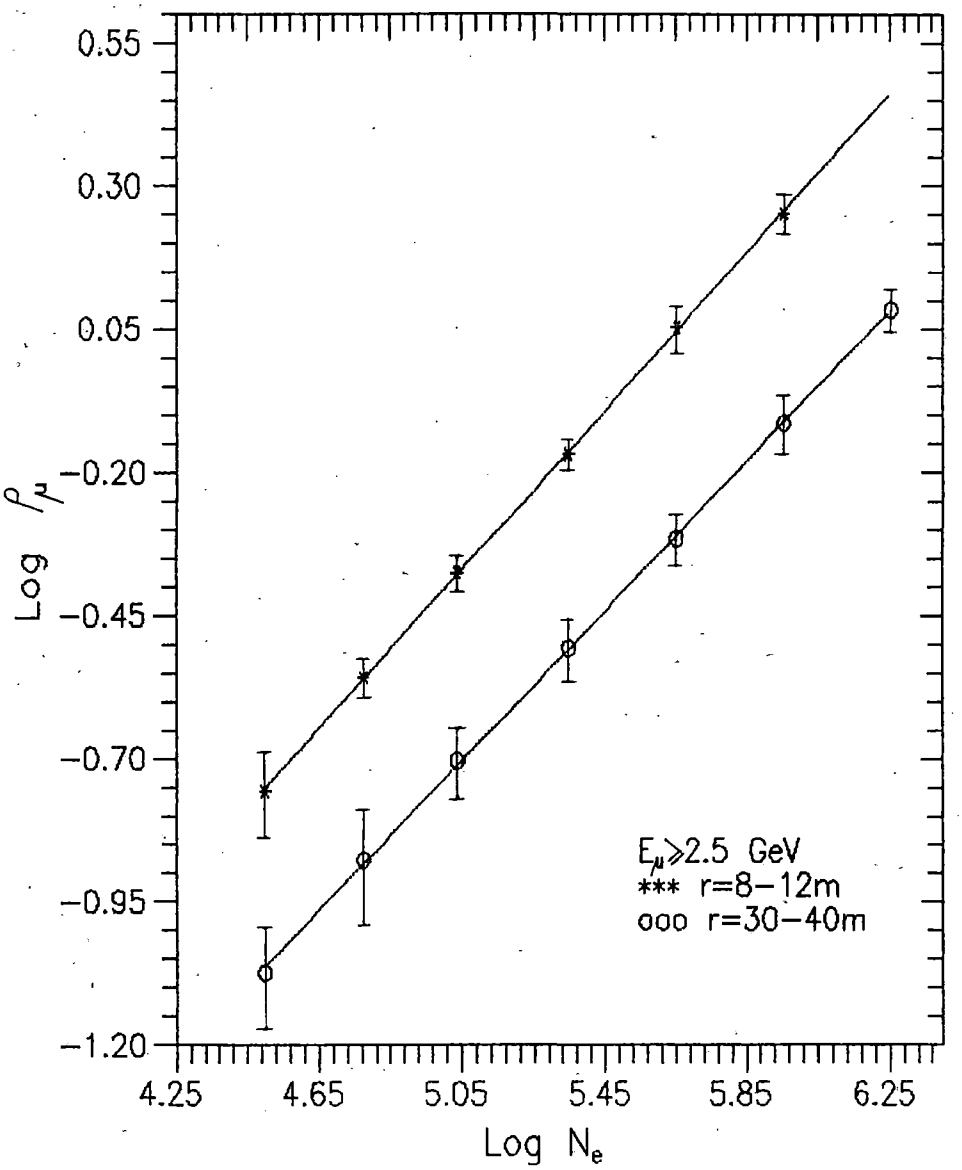
0.55
0.30
0.05
−0.20
−0.45
−0.70
−0.95
−1.20
Log ρ_μ
4.25
4.65
5.05
5.45
5.85
6.25
Log N_e
$E_\mu \geq 2.5$ GeV
*** r=8−12m
ooo r=30−40m

Fig.11

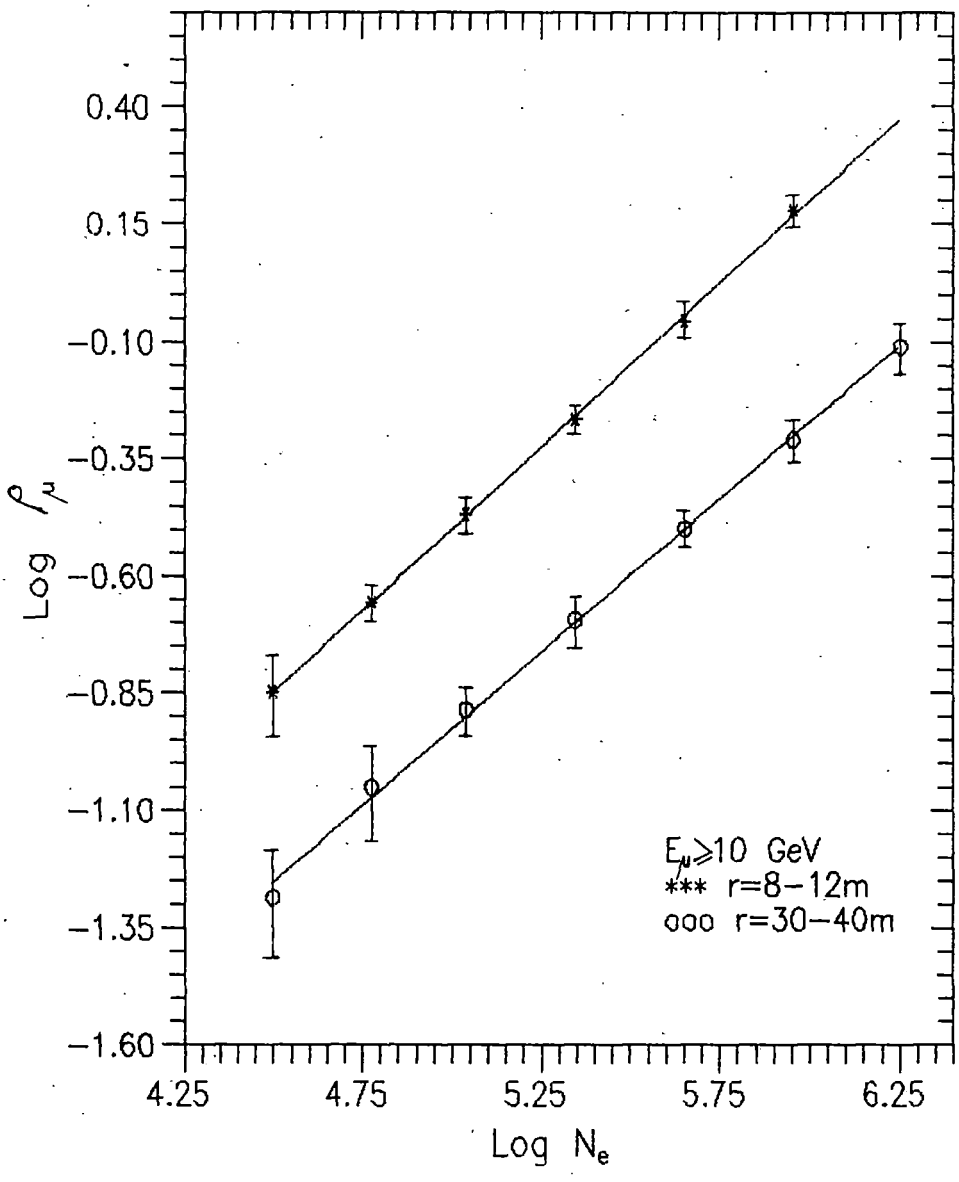
0.40
0.15
−0.10
−0.35
−0.60
−0.85
−1.10
−1.35
−1.60
Log ρ_μ
4.25
4.75
5.25
5.75
6.25
Log N_e
$E_\mu \geq 10$ GeV
*** r=8−12m
ooo r=30−40m

Fig.12

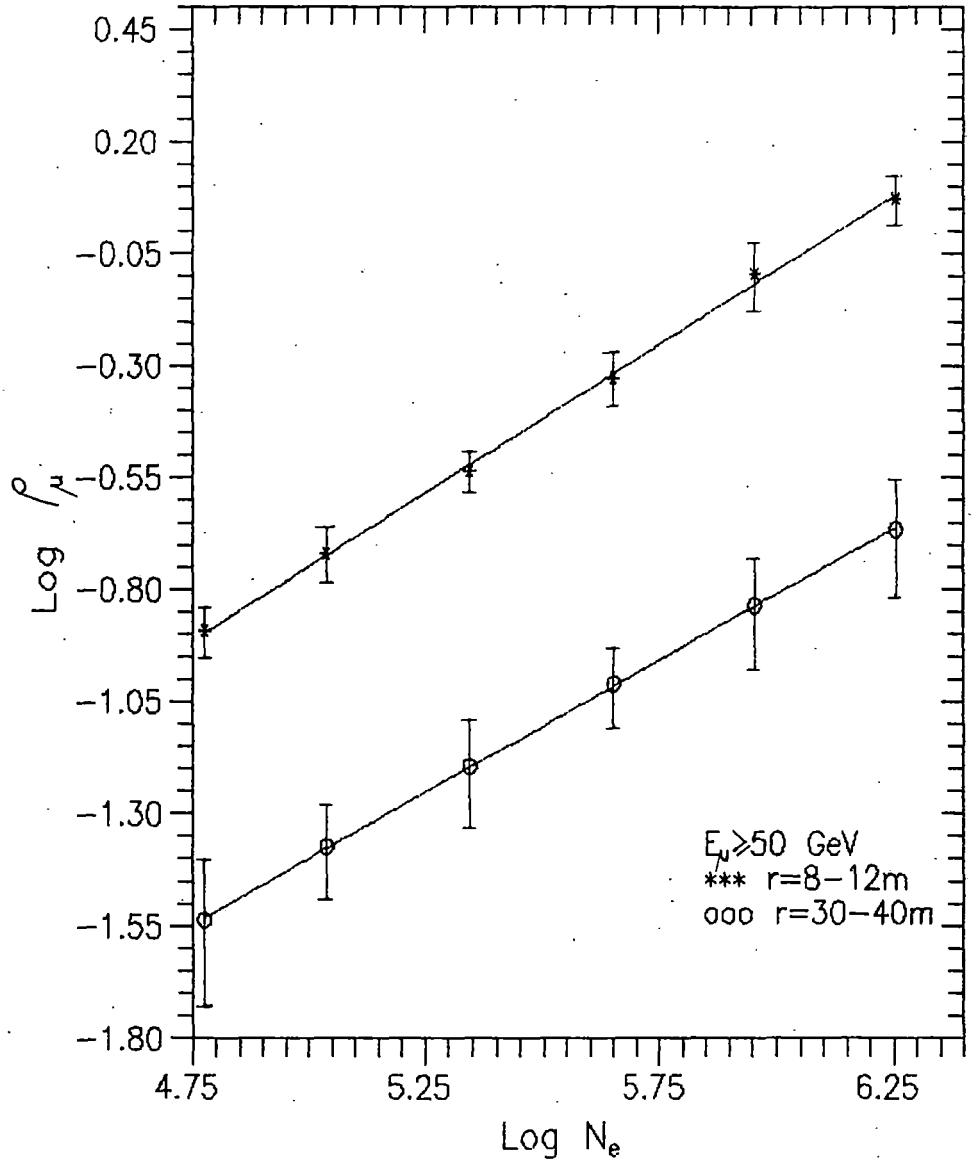
0.45
0.20
−0.05
−0.30
−0.55
−0.80
−1.05
−1.30
−1.55
−1.80
Log ρ
4.75
5.25
5.75
6.25
Log N_e
E_γ≥50 GeV
*** r=8−12m
ooo r=30−40m

Fig.13

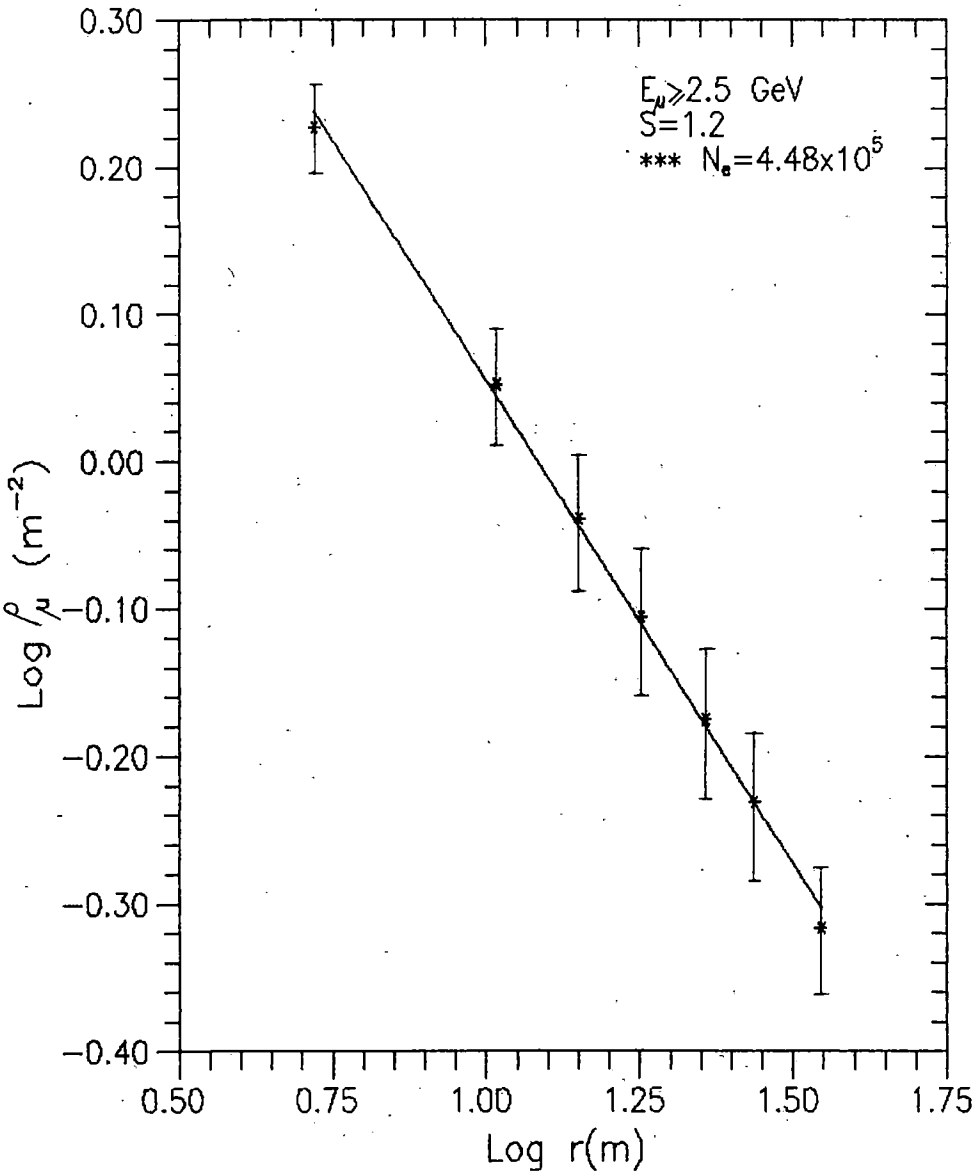
$E_\mu \geq 2.5$ GeV
S=1.2
*** $N_e = 4.48 \times 10^5$
0.30
0.20
0.10
0.00
−0.10
−0.20
−0.30
−0.40
Log ρ_μ (m^{-2})
0.50
0.75
1.00
1.25
1.50
1.75
Log r(m)

Fig.14

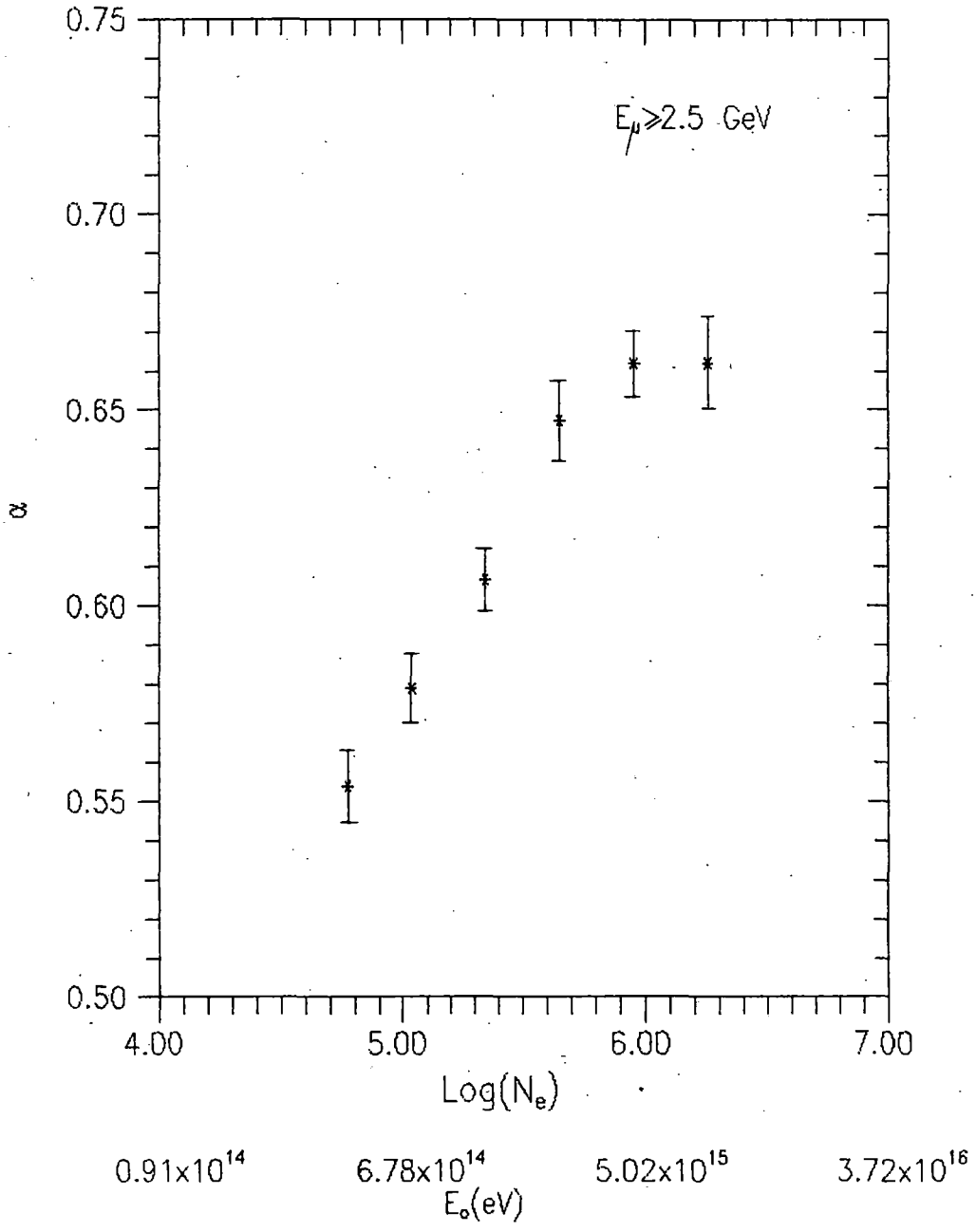
0.75
0.70
0.65
0.60
0.55
0.50
α
$E_\mu \geq 2.5$ GeV
4.00
5.00
6.00
7.00
Log(N_e)
0.91×10^{14}
6.78×10^{14}
5.02×10^{15}
3.72×10^{16}
E_o(eV)

Fig.15